

Qualification of the FFT spectrometer Phoenix-3

Christian A. Monstein, Hansueli Meyer, Andreas James

ETH Zurich, Institute of Astronomy, CH-8092 Zurich, Switzerland

Draft 14.11.2007 / Updated 01.04.2009

Abstract. Phoenix-3 based on a commercially available FFT spectrometer board AC-240, connected to a broadband receiver was qualified to be used as a solar polarization spectrometer. A pile of very time consuming measurements showed, that the system fulfills the given requirements to observe solar radiation between 1GHz and 5GHz in two polarizations. The total of 65536 channels produces 65 times more data compared to the existing 1000 channels of Phoenix-2. The total bandwidth is comparable with Phoenix-2 but time resolution is much better than Phoenix-2. The radiometric sensitivity is also slightly better than Phoenix-2 due the fact that all samples are integrated on board of the FFT - FPGA.

Key words. Allan time, SFDR, Bandwidth, Y-factor, Noise Figure, Calibration, Data compression.

1. Introduction

The new FFT spectrometer Phoenix-3, developed in 2006 until 2007 is the successor of the frequency agile spectrometer Phoenix-2. The Phoenix-3 spectrometer needs to be qualified with respect to the specification and the statement of work. This qualification includes all the hardware from the antenna via the FPU, receiver to the backend including all associated software processes for cleaning, integration, filtering and compression of the observed data. All necessary measurements were done at Bleien observatory using existing tools and methods.

Different acronyms used in labels and text are described in table 6.

2. Double heterodyne receiver

Phoenix-3 receiver is a double heterodyne instrument with $4 \times 1\text{GHz} = 4\text{GHz}$ bandwidth. Four local oscillators of 4GHz, 5GHz, 6GHz and 7GHz shift the incoming rf band upwards to 8GHz where the first IF filtering and main amplification takes place. An extra local oscillator of 8GHz shifts this IF down to zero into the baseband to be fed into the FFT hardware. Schematics are given in sketches fig. 2 until 4. All components are commercially available but about 80% was bought through eBay to save money.



Fig. 1. Phoenix-3 receiver 1-5GHz for two polarizations top left, FPU-controller top right, FFT spectrometer ARGOS bottom left (green box) and FTP-server PERISCOPE bottom right at Bleien observatory, about 50 km south of Zurich.

3. Qualification measurements

All qualification measurements were done at the observatory site in Bleien using well known procedures, tools and methods. Most of the results are based on the measurement of the quiet sun of November 7th 2007. Transit measurements originate from November 20th 2007.

3.1. Warm up time

Warm up time is defined as the time where all effects due to internal temperatures of the components like pream-

Double Heterodyne Receiver stage 1

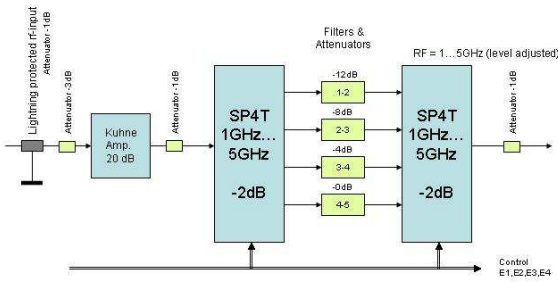


Fig. 2. Lightning protection, gain equalization and input filtering of Phoenix-3 heterodyne receiver.

Double Heterodyne Receiver stage 3

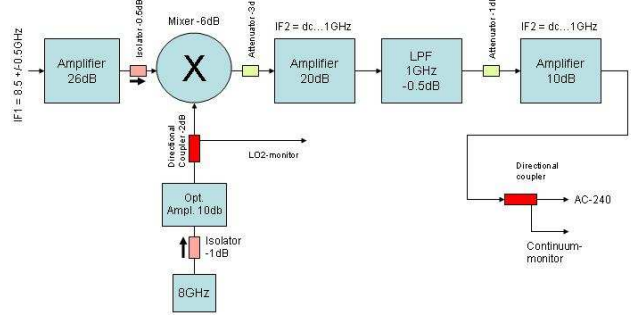


Fig. 4. Second mixer stage and low pass filtering of Phoenix-3 heterodyne receiver.

Double Heterodyne Receiver stage 2

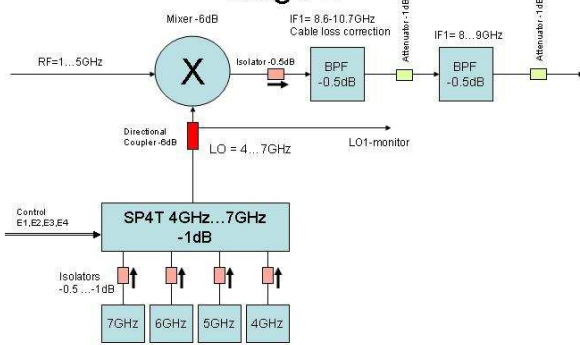


Fig. 3. First mixer stage and IF filtering of Phoenix-3 heterodyne receiver.

plifiers, LO's mixers, FPGA etc. have reached more than 95% of their final value. This time should be taken into account when doing calibrated measurements, allan time measurements or analyzing drift curves. In our case warm up time is at least $tw \geq 15minutes$, see figure 5.

3.2. Allan time

Allan time describes how long we are allowed to integrate without re-calibration. This test will be done by observing different sources, namely the sun, cold sky position and a termination resistor. This, to distinguish between artifacts from antenna positioning system and receiver.

3.2.1. Allan time while pointing to then sun

This represents the worst case scenario including antenna positioning errors and outside rfi. Although originally planned, this time consuming measurement and analysis procedure is useless due to changing flux of the source rfi.

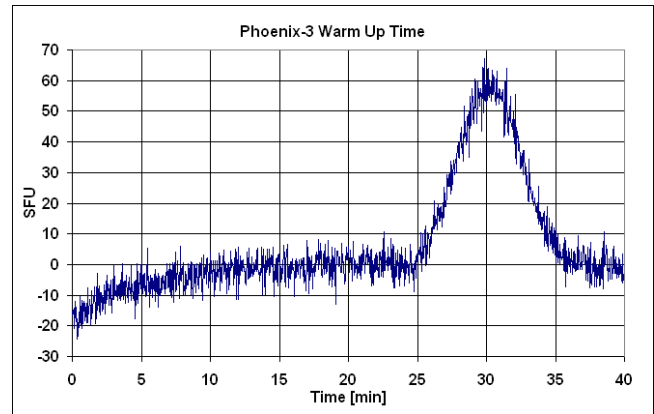


Fig. 5. Warm up time of the complete system after switching it on. Data shown are for one polarization which were calibrated for quiet solar flux of $S = 112sfu/2 = 56sfu$. From 25min until 35min a sun transit at 4613MHz takes place.

3.2.2. Allan time while pointing to cold sky

All influences of antenna pointing system disabled but including outside rfi. Although originally planned, this time consuming measurement and analysis procedure is also useless due to changing flux of the source and rfi.

3.2.3. Allan time while observing termination resistor

All influences of antenna pointing system and outside rfi disabled thus, it makes sense to measure and analyze this because the test can be repeated every time needed under controlled condition. For single frequency results, see figures 6, 7 and 8.

3.3. Spectrum of quiet sun

Spectrum of quiet sun shown in fig. 9 shall give an impression about the general level and swr of sky background and sun noise in all bands for left hand polarization LHCP. This set of data is used for the evaluation of the Y-factor,

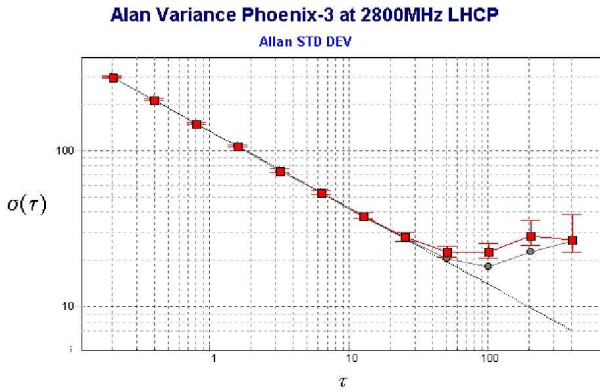


Fig. 6. Allan time of T0 in LHCP is better than 100 seconds at 10cm wavelength and almost identical to RHCP.

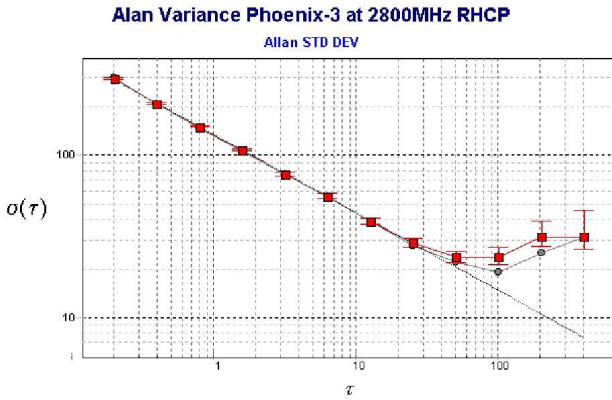


Fig. 7. Allan time of T0 in RHCP is better than 100 seconds at 10cm wavelength and almost identical to LHCP.

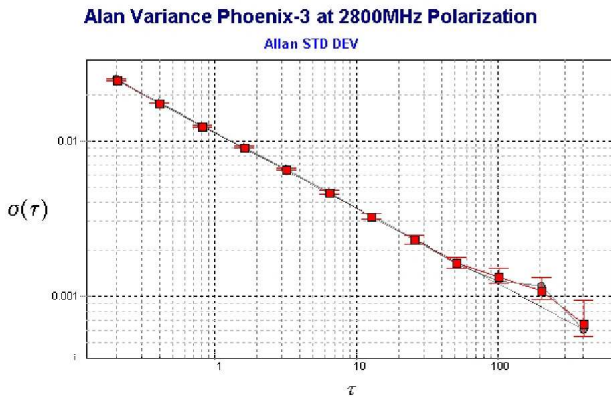


Fig. 8. Allan time of polarization $100 \cdot (LHCP - RHCP)/(LHCP + RHCP)$ is better than 5 minutes at 10cm wavelength.

SNR, receiver noise etc. Spectrum of quiet sun shown in fig. 10 shall give an impression about the general level and swr of sky background and sun noise in all bands for right hand polarization RHCP. Also this set of data is used for the evaluation of the Y-factor, SNR, receiver noise etc.

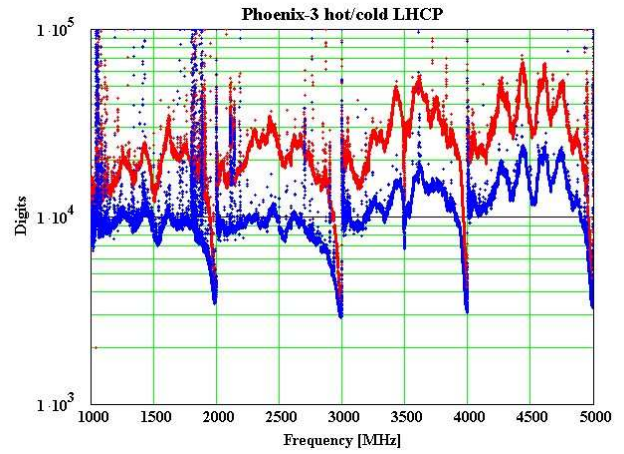


Fig. 9. Stored digital values (raw data) of the quiet sun for all bands (65536 channels) in left hand circular polarizations, red for on-sun- and blue for off-sun-position.

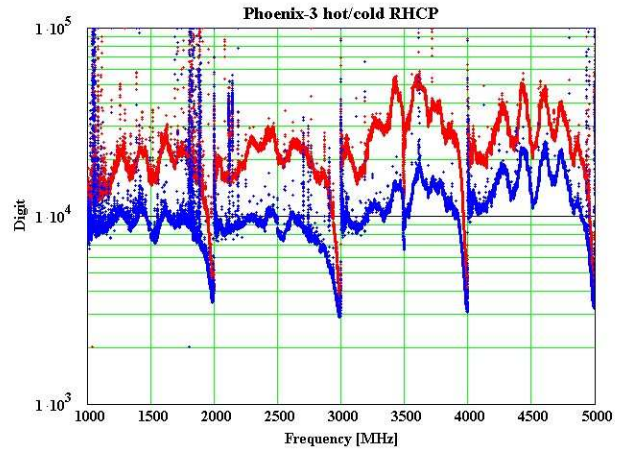


Fig. 10. Stored digital values (raw data) of the quiet sun for all bands (65536 channels) in right hand circular polarizations, red for on-sun- and blue for off-sun-position.

3.4. Y - factor

The so called Y-factor is defined as the fraction of on-sun signal divided by off-sun signal. It is an ideal mean for a first check of the system quality. It should be checked regularly once or twice a year. Every bad cable, connector or simply any pointing error of the antenna leads to a bad Y-factor. Plots for all bands and polarizations are shown in fig. 11, Y-factor for intensity (LHCP+RHCP) expressed in dB is shown in fig. 12.

3.5. Beam angle

The beam angle ϕ is needed to estimate directivity D , gain G and efficiency η of the antenna system. A meridian transit of quiet sun was used to get the transit plot for all bands in intensity in the direction of hour angle α . The analysis of Δt in fig. 13 shows an angular beam width of:

$$\varphi = 15^\circ / h * \Delta t \cos(\delta) = 0.88^\circ \quad (1)$$

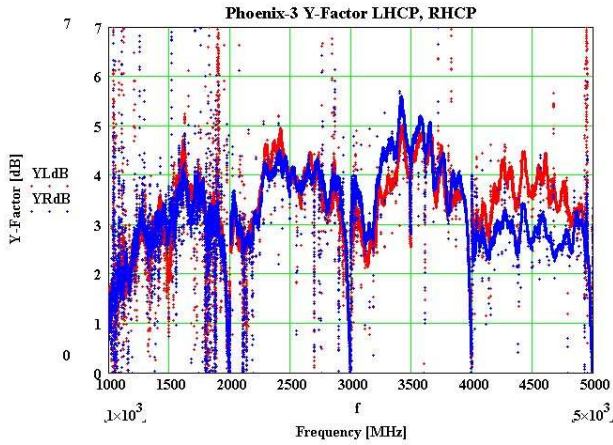


Fig. 11. Y-factor of the quiet sun for all bands (65536 channels) in both polarizations, red for LHCP and blue for RHCP.

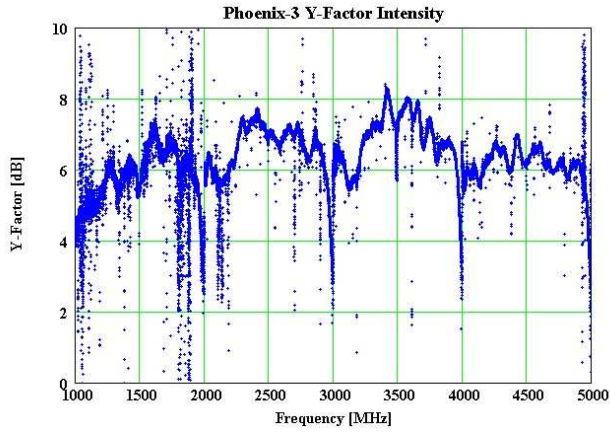


Fig. 12. Y-factor in intensity of the quiet sun for all bands (65536 channels).

with $\delta = -20^\circ$ on 20th of November 2007. Just to compare with theory, the beam angle should roughly be

$$\varphi = 1.22 \frac{\lambda}{D} = 0.91^\circ \quad (2)$$

which fits quite good with the measurement in eq. 1

3.6. Antenna directivity

To get antenna directivity D , every light curve (for example, see fig. 13) has to be normalized between 0 and 1 and then integrated over full hour angle of a meridian transit. The result squared denotes to beam solid angle Ω_a .

$$\Omega_a = \left[\sum_{i=0}^{N-1} \frac{y_i - \min(y) - pp/2}{\max(y) - \min(y) - pp} d\alpha \right]^2 \quad (3)$$

where $d\alpha$ denotes to measurement increment in time dt expressed as angle where $dt = 2sec$ in our case. And N denotes to the number of pixels per spectrum, $N = 65536$. Variable pp denotes to peak-peak value of lightcurve while pointing to cold sky. It is needed to better normalize the

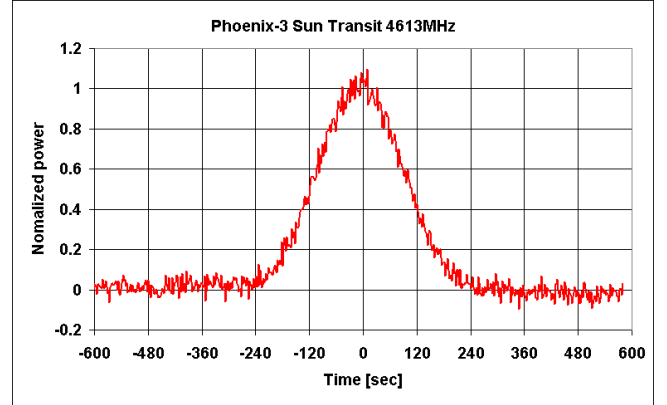


Fig. 13. Example of a normalized (in time and amplitude) transit light curve at 4613MHz, bandwidth 60KHz, integration time 125msec, LHCP only.

lightcurves. Variable $\min(y)$ and $\max(y)$ denote to minimum respective maximum of the whole array of every lightcurve. Ω_a has to be computed separately for both polarizations. I assume that the east-west pattern is identical to north-south pattern, this to reduce measurement and analysis time.

$$d\alpha = \frac{dt}{3600sec/h} \frac{360^\circ}{24h} \cos(\delta) \quad (4)$$

Beam solid angle Ω_a compared with full sky of 4π leads to directivity D .

$$D = \frac{4\pi}{\Omega_a} \left[\frac{180^\circ}{\pi} \right]^2 \quad (5)$$

3.7. Antenna gain

To get antenna gain G from directivity D given in 5, one just needs to take the logarithm according to eq. 6. I don't take into account effects of side lobes, spillage etc., all analysis steps are done for the main beam only.

$$G_{dB} = 10 \log(D) \quad (6)$$

We may compare measured gain, shown in fig. 14 with basic antenna theory given in eq. 7

$$G_{dB} = 10 \log \left[\eta \left[\frac{d \pi}{\lambda} \right]^2 \right] \quad (7)$$

where η denotes to aperture efficiency, d to dish diameter and λ to receiving wave length. Antenna gain was evaluated by numeric integration of normalized beam pattern over hour angle of a meridian transit through quiet sun.

3.8. Effective area

Effective area is computed from directivity using eq. 8 for all bands and both polarizations. Plots for both polarizations and all bands are shown in fig. 15. Effective area is not as good as it could probably be due to some pointing

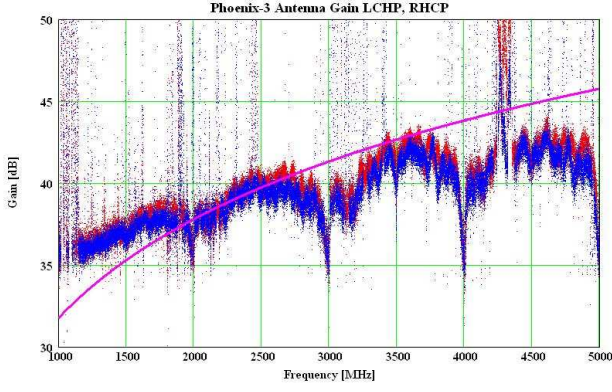


Fig. 14. Measured gain in both polarizations for all bands (2×65536 channels). The solid line (purple) shows the theoretical gain (see eq. 7) assuming, the antenna efficiency is $\eta = 0.55$ and dish diameter is $d = 5m$. Pixel plot LHCP in red, RHCP in blue.

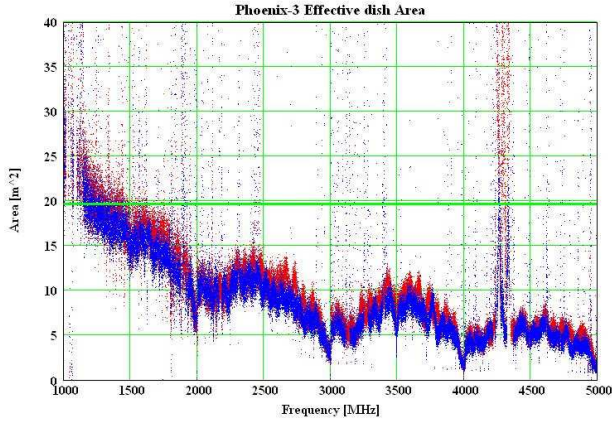


Fig. 15. Effective area of 5m dish in both polarizations for all bands (2×65536 channels). A solid line (green) shows the geometrical area. Pixel plot LHCP in red, RHCP in blue.

error during observation in the afternoon. Also interference from ground and sides lobes which are looking into ground were not taken into account.

$$A_{eff} = \lambda^2 \frac{D}{4\pi} \quad (8)$$

where D denotes to directivity of the antenna system.

3.9. Efficiency factor

Efficiency factor expressed in % and plots for all bands and polarizations are shown in fig. 16. The values are computed from previous results.

$$\eta = \frac{A_{eff}}{\pi r^2} \quad (9)$$

where r denotes to the radius of the parabolic dish antenna.

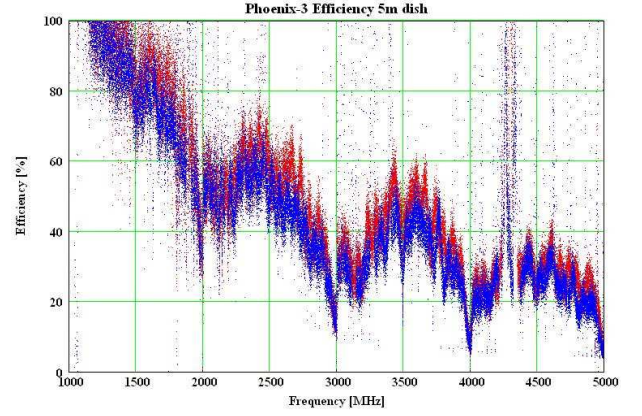


Fig. 16. Efficiency of 5m dish in both polarizations for all bands (2×65536 channels) Pixel plot LHCP in red, RHCP in blue.

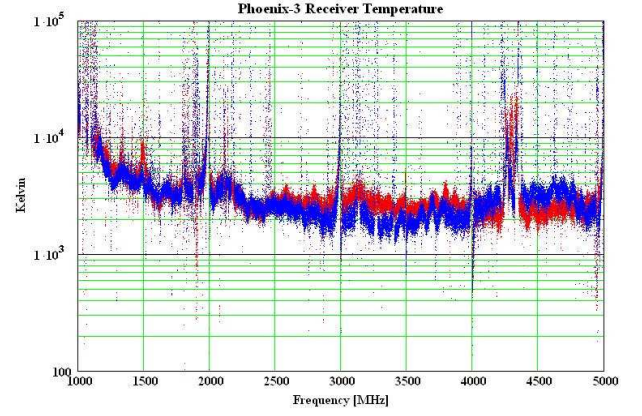


Fig. 17. System temperature of 5m dish in both polarizations for all bands (2×65536 channels). Pixel plot LHCP in red, RHCP in blue.

3.10. System temperature

Receiver temperature is computed from several results above (Y-factor, quiet sun, effective area). Plots for all bands and both polarizations are shown in fig. 17.

$$T_{a_{sun}} = \frac{S_{sun} A_{eff}}{2k} \quad (10)$$

and

$$T_{sys} = \frac{T_{a_{sun}}}{Y_{sun} - 1} = \frac{S_{sun} A_{eff}}{2k(Y_{sun} - 1)} \quad (11)$$

S_{sun} denotes to flux of radio quiet sun and k to Boltzman constant. Equations 10 and 11 have to be applied to each polarization individually.

3.11. Noise figure NF

Noise figure is computed from system temperature (see figure 17) and a reference temperature which is defined as $T_{ref} = 290K$, see eq. 12. Plots for all bands and polarizations are shown in fig. 18.

$$NF = 10 \log \left[\frac{T_{sys}}{T_{ref}} \right] \quad (12)$$

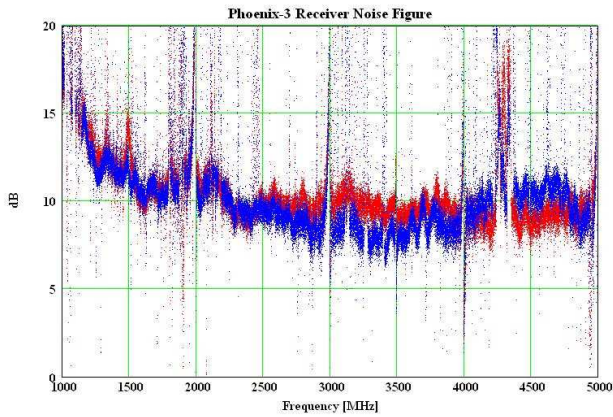


Fig. 18. Noise figure [dB] of complete receiving system in both polarizations for all bands (full spectral resolution with 2×65536 channels). Pixel plot LHCP in red, RHCP in blue.

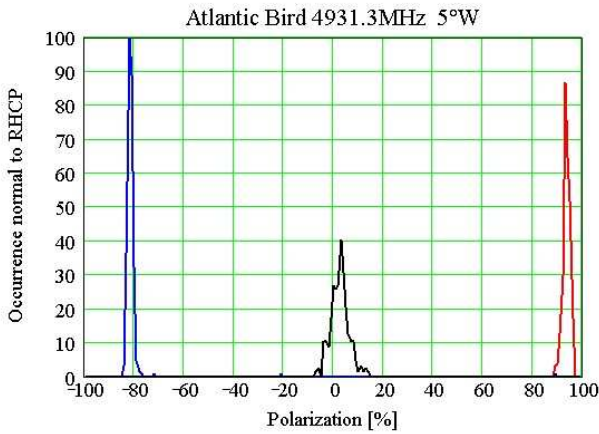


Fig. 19. Both polarization signals of Atlantic Bird satellite at geostationary position $5^\circ W$ at $4931.2 MHz$ compared to an unpolarized signal from sky. Pixel plot RHCP in red, LHCP in blue, unpolarized in black.

where log means log to the base of ten. NF is expressed in dB.

3.12. Polarization test on satellites

Geostationary satellites with well defined polarization of their down link transmitters or beacons are ideal to check polarization measurement and calibration procedure. Satellite beacons should show polarization in the order of nearly $\pm 100\%$ minus cross coupling in the order of $-20 dB$ (-1%). While other satellites like METEOSAT with linear polarization should show 0% circular polarization. It is also an easy way to find out the sign for LHCP and RHCP.

3.12.1. Sign of polarization

To find out the sign of polarization we have been observing the geostationary communication satellite INMARSAT-2F2 at satellite position $15.5^\circ West$. From its specification,

Polarization	Average [%]	Standard deviation [%]
RHCP	+93.5	1.4
LHCP	-81.1	5.4
no	+2.8	5.9

Table 1. Average polarization and standard deviation for LHCP, RHCP and unpolarized channels of Atlantic Bird satellite.

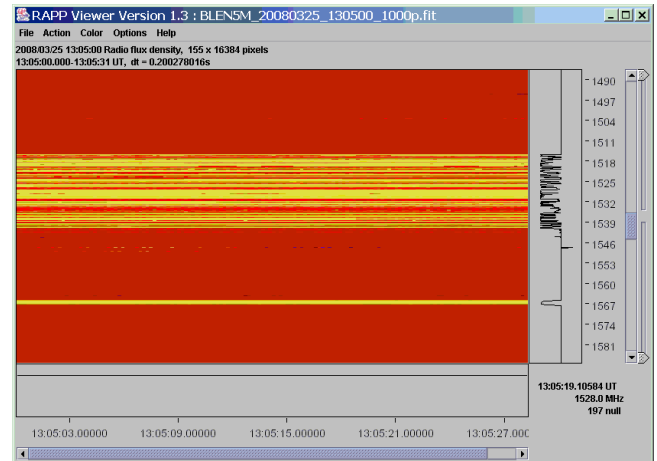


Fig. 20. Polarization-Spectrum from Inmarsat satellite at geostationary position $15.5^\circ W$ in L-band during a few seconds of observation. All have the same RHCP-polarization.

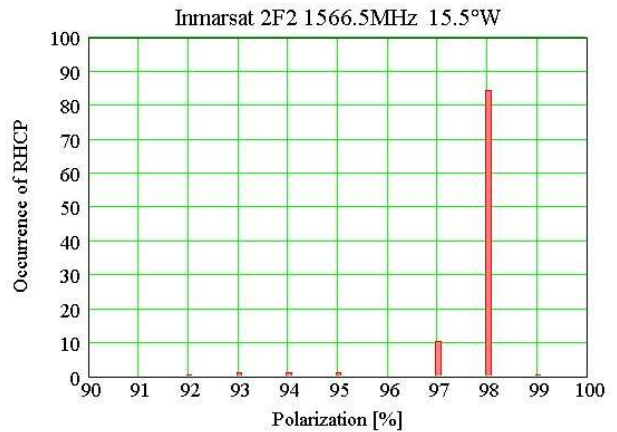


Fig. 21. RHCP channel statistics from Inmarsat satellite at geostationary position $15.5^\circ W$ in L-band during a few seconds of observation.

we know that all channels in L-band are RHCP, see figure 20. In figure 21 we see a statistic about the distribution of the polarization in time.

3.13. Beam power pattern

By letting the antenna system do a raster fly map or a so called scan field, one can gain a set of data to produce a beam power pattern which, in fact, is the convolution of the real beam power pattern with suns disc. The scan parameters were as follows: $\Delta \angle = \pm 2.2^\circ$,

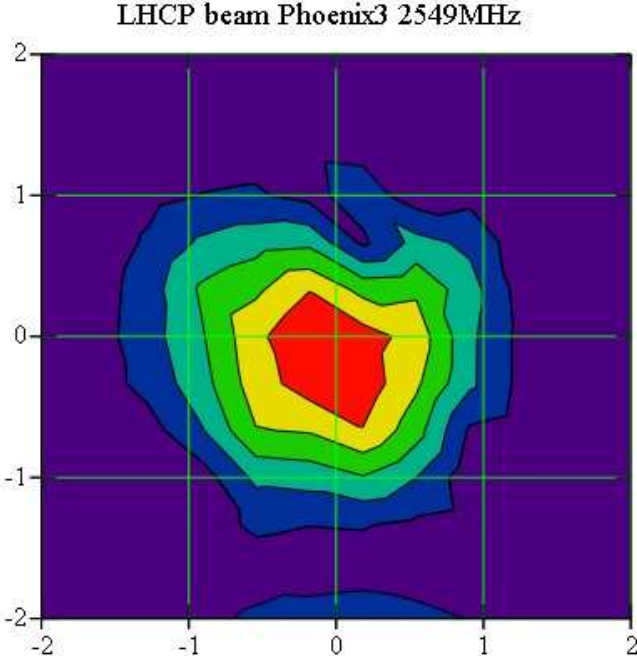


Fig. 22. Beam power pattern at 2549MHz for left hand circular polarization. Pointing error in azimuth and elevation $< 0.2^\circ$.

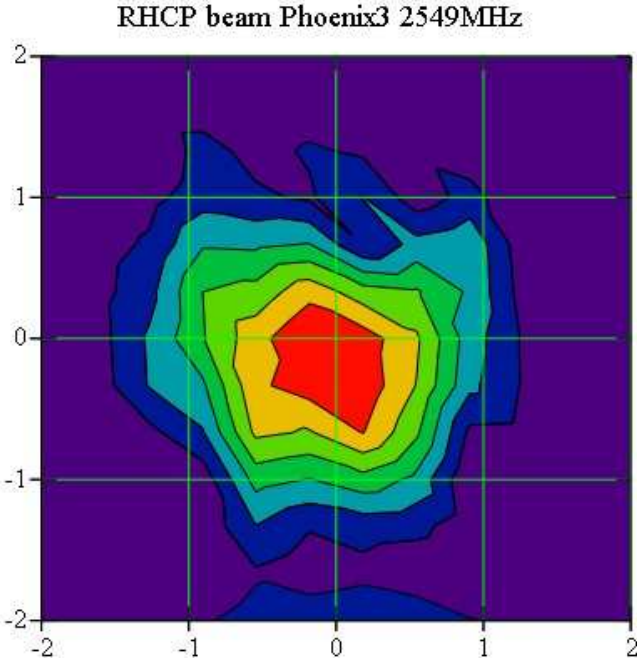


Fig. 23. Beam power pattern at 2549MHz for right hand circular polarization. Pointing error only in elevation of $< 0.2^\circ$

$\Delta \text{elevation} = 0.1^\circ$, speed $v = 0.12^\circ/\text{sec}$. Integration time was increased from 12.5msec to 125msec per pixel while the time resolution for a full spectrum was 2sec . For plots in both polarizations, see figures 22 and 23.

3.14. Dynamic range

All bands and all polarizations are suffering from a reduction of DR due to standing waves SWR and gain slopes

Band	maximum value and unit
1GHz - 2GHz	$< \pm 1.7\text{dB}$
2GHz - 3GHz	$< \pm 1.1\text{dB}$
3GHz - 4GHz	$< \pm 1.4\text{dB}$
4GHz - 5GHz	$< \pm 0.8\text{dB}$

Table 2. Maximum standing waves in intensity-Y-factor, including slope per receiver band.

Band	MHz	$\sigma[\text{sfu}]$	$\bar{x}[\text{sfu}]$	$\tau[\text{sec}]$	$\sigma_\tau[\text{sfu}]$
1 - 2 GHz	1421	0.97	70.7	3	< 0.3
2 - 3 GHz	2695	0.98	97.4	3	< 0.3
3 - 4 GHz	3414	1.55	120.9	2	< 0.4
4 - 5 GHz	4850	2.36	153.9	3	< 0.7

Table 3. Sensitivity per band in intensity while observing quiet sun in non compressing mode. σ denotes to standard deviation within 1200 pixels (4 minutes of observation). \bar{x} denotes to average solar flux [sfu]. Time τ denotes to Alan time and σ_τ to one sigma in flux after integration according to Alan time.

given in table 2. Special filters were switched in to compensate for gain slope.

3.15. Spurious free dynamic range SFDR

all bands in intensity only (dB) to be measured...

3.16. Sensitivity

Sensitivity was analyzed using real data of November 12th 2007 while observing quiet sun. Only one single frequency was analyzed, per GHz-band due to very time consuming analysis processes. Selected frequencies are all either reserved for radio radio astronomy or transmission is prohibited in Switzerland. Results without any compression in FITS-files are listed in table 3, while per default compressed data are listed in table 4. In general, sensitivity is most probably limited by the bad antenna positioning system (mechanics, electronics and software) and also bad numerical resolution.

3.16.1. Non compressed FITS

Just for comparative analysis data were directly stored in the FITS files without any compression algorithm, see table 3. This mode should only be used for quiet sun or spectral line observations but not for observations of dynamic flares.

$$\text{FITS} = \text{int}(\text{sfu} + 0.5) \quad (13)$$

Maximum flux is limited in this mode to $S_{\text{max}} \leq 255 \text{ sfu}$ in all bands.

Band	MHz	σ [sfu]	\bar{x} [sfu]	τ [sec]	σ_τ [sfu]
1 - 2 GHz	1421	0.95	70.9	3	< 0.4
2 - 3 GHz	2695	1.03	97.1	3	< 0.2
3 - 4 GHz	3414	1.59	120.2	3	< 0.2
4 - 5 GHz	4850	2.52	152.7	3	< 0.2

Table 4. Sensitivity per band in intensity while observing quiet sun in logarithmic compressing mode. σ denotes to standard deviation within 1200 pixels (4 minutes of observation). \bar{x} denotes to average solar flux [sfu]. Time τ denotes to Alan time and σ_τ to one sigma in flux after integration according to Alan time.

Band	Fmin/MHz	Fmax/MHz	Yield
1 - 2 GHz	1017	1966	94.9%
2 - 3 GHz	2000	2968	96.8%
3 - 4 GHz	3006	3971	96.5%
4 - 5 GHz	4000	4978	97.8%

Table 5. Bandwidth (-3dB) of each band in intensity, analyzed from Y-factor.

3.16.2. Log compressed FITS

Standard compression of measured data to cope on one hand with intensive flares and on the other hand with 8bit data format of our standard FITS files. For statistical results, see table 4. This mode is the default mode for solar observations, but can not be used for non-solar observations.

$$FITS = 70 \log(sfu - 50) \quad (14)$$

Maximum flux is limited in this mode to $S_{max} \leq 4444$ sfu in all bands.

3.17. Bandwidth

Useable bandwidth for each GHz-band at $-3dB$ analyzed from Y-factor in intensity, see table 5. Yield factor could be improved by 1 to 2 percent by optimizing the low pass filter to more than standard 5 poles. But this would need an investment in the order of 10 kFr.

3.18. Channel width

Channel width of one single channel ($-3dB$, $-10dB$) was analyzed by applying an external rf-signal generator with programmable frequency and power. The -3 dB bandwidth was found to be 97.5 ± 1 kHz. The -10 dB width was found to be 180.0 ± 1 kHz. And the attenuation of the first order wing was found to be better than -29.0 dB.

3.19. Window function

In another investigation it was found out, that Blackman windowing $w[n]$ is best for solar radio astronomy in a

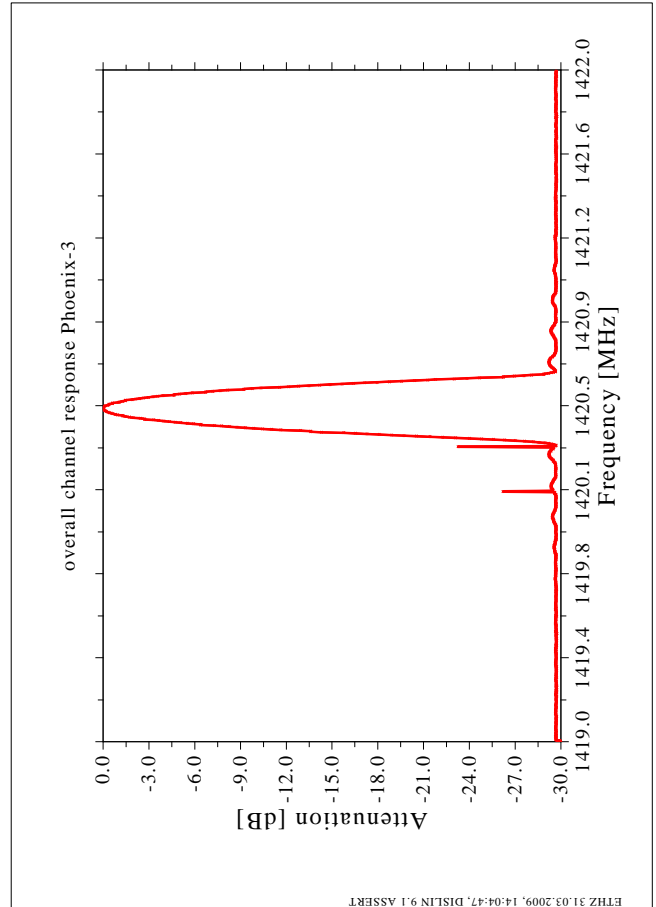


Fig. 24. Channel response of Blackman filter to an external cw signal fed into the antenna input of the receiver. Small peaks are due to numerical limitations within the FPGA.

strong rfi polluted environment, see eq. 15 and fig. 25 for plot. An extra paper (Meyer, 2007) was published recently in e-collection.

$$w[n] = a_0 - a_1 \cos\left(\frac{2\pi n}{N-1}\right) + a_2 \cos\left(\frac{4\pi n}{N-1}\right) \quad (15)$$

where n denotes to the pixel address in the sampled data array and N to the number of pixels, which in our case is 2×16384 . Constants $a_0 = 0.42$, $a_1 = 0.5$, $a_2 = 0.08$ are for Blackman window.

3.20. Calibration

Every change in the hardware- or software configuration has to be taken into account by doing a re-calibration. Calibration in this case means the following. - measure quiet sun at noon for at least 4 minutes. - move antenna to cold sky position about 180degree azimuth and 70degree elevation. - measure cold sky for at least 4 minutes. - Move all raw-files to the server periscope into drive which is foreseen for calibration tool. Load and run the application 'raw2fitscal.exe' in local directory 'RAW2FitsCalibrationPhoenix3' and move the resulting calibration file 'Phoenix3Calipar.prn' into data/cali. The file 'Phoenix3CaliPar.prn' is composed of 5 columns,

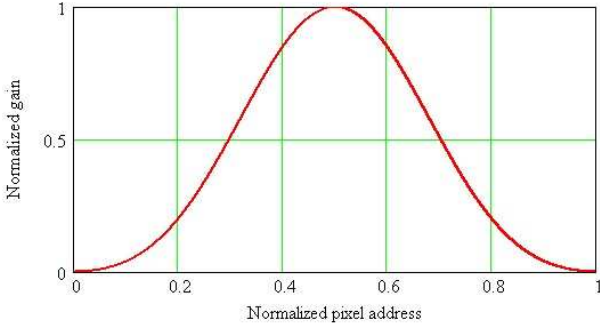


Fig. 25. Blackman window function to cope with high level radio frequency interference from nearby transmitters (mobil phone, pager etc.).

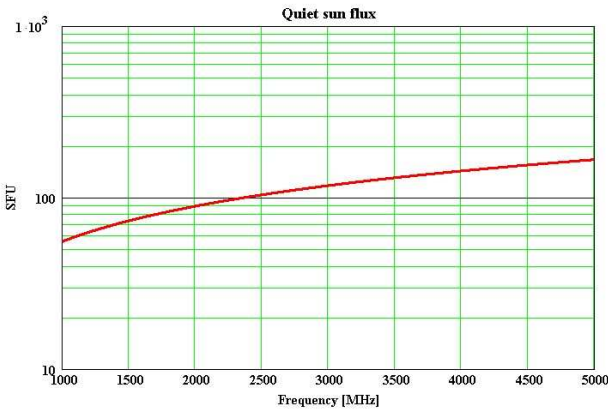


Fig. 26. Theoretical model of solar flux after Smerd and Kundu 1965.

65536 rows long containing frequency in MHz, actual sun flux in sfu according to equations 16 until 20, cold sky for LHCP, cold sky for RHCP, sun for RHCP and sun for LHCP. Solar flux for quiet sun in range 300MHz until 11'200MHz (which was calculated after models from Smerd and Kundu p.117 of 1965), is

$$S_q = 0.50 f^{0.682} \quad (16)$$

and in lower range from 63MHz up to 300MHz

$$S_q = 2.07 \cdot 10^{-4} f^{2.047} \quad (17)$$

for slowly varying sun between 2770MHz and 10'000MHz after Kundu p. 170 of 1965, we get

$$\Delta S = 35.12 f^{-0.5045} \quad (18)$$

and for slowly varying sun until 2'770MHz we get

$$\Delta S = 1.20 \cdot 10^{-5} f^{1.374} \quad (19)$$

Total flux is the sum of quiet sun plus slowly varying sun.

$$S = S_q + \Delta S Z \quad (20)$$

where Z denotes to actual sunspot number. All results expressed in sfu and frequencies in MHz. For plot, see fig. 26

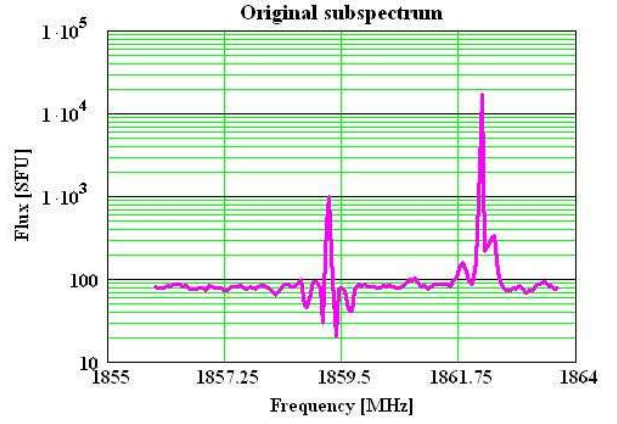


Fig. 27. Example of a subspectrum in the mobile phone frequency range at 1860MHz with a lot of radio interference. Positive peaks are due to radiation during measurement, negative peaks due to radiation during previous calibration process.

3.21. Data reduction

To cope with limited transfer speed of the ADSL cable to Zurich and with limited disk capacity at the observatory and the institute we have to reduce the amount of data. Also to cope with existing analysis tools it makes sense to keep files small. One single raw file for 1GHz bandwidth in full resolution for 4 minutes needs 80MByte of data! Data reduction is thus done in three steps. First after calibration a filter process is applied to get rid of rfi. Secondly the remaining data are integrated, typically by a factor of 32, 64 or even 128. These filtered and integrated data are then compressed into 1 of 3 possible schemes and written to a FITS file.

3.21.1. Filter process

Filter process is just a statistical analysis of the spectrum. The spectrum is divided into N subspectra, where N is in the order of 32, 64 or 18. For a typical subspectra, see fig. 27. Each subspectrum is then sorted in ascending order. For a typical sorted subspectrum, see fig. 28. Now the assumption is, that we may expect the median value at $N/2$. And we define a so called waste factor w in the order of $\pm 10\% \dots \pm 30\%$. This waste factor is used to throw away sorted data at the left- and right border of the sorted subspectrum. The remaining spectral data points represent the most probable value as an average at the center frequency of the subspectrum.

3.21.2. Numerical integration

All remaining data points of the subspectrum are numerical integrated to one single value at the center frequency of the subspectrum, see eq. 21

$$\sum_{k=n1}^{n2} \frac{y^{sk}}{n2 - n1} = 82.192 \text{ sfu} \quad (21)$$

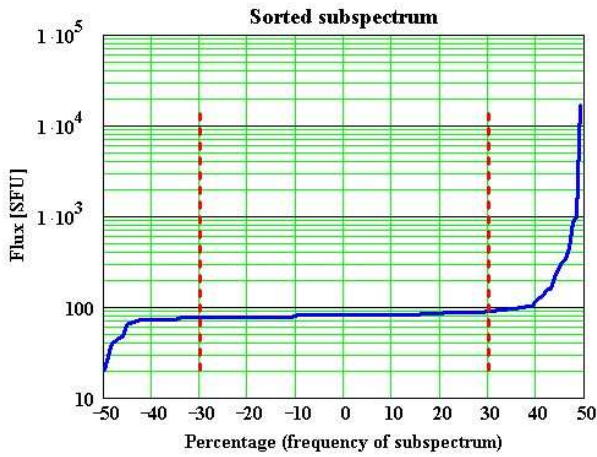


Fig. 28. Subspectrum sorted in ascending order. Vertical dashed lines (red) denote to the integration limits. Only data between these two lines are integrated, all the rest is skipped. In this example the waste factor w is $\pm 30\%$

where $n1$ denotes to the left starting point of the integration and $n2$ to the right one, marked by red dashed lines in fig. 28

3.21.3. Compression

There are three rather different compression algorithms available. The main idea is to keep the amount of data as low as possible. In this case we try to stay with the 8bit-format of the FITS files (type BYTE).

$$FITS = int(sfu + 0.5) \quad (22)$$

The easy way given in Eq. 22 to directly store flux units in the file with the advantage of 1sfu resolution and disadvantage to be limited to 255sfu.

$$FITS = 45 \log(sfu + 10) \quad (23)$$

Eq. 23 shows the traditional way of compression algorithm inherited from the Phoenix-2 era.

$$FITS = 70 \log(sfu - 50) \quad (24)$$

Eq. 24 shows a new way to cope with calibrated data to get a resolution as high as possible and maximum flux of $S_{max} \leq 4444sfu$ for unpolarized signals.

4. Conclusions

Here conclusions

Acknowledgements. I thank Frieder Aebersold for perfectly milling the modul-, front- and back-plates. Serge Zihlmann for mechanical work at the focal plane unit, FPU-controller and receiver. NF grant xyz.

5. Relevant internet addresses

url1: Daten Phoenix-3 url2: Webseite mit Spiegel

Abbreviation	description
AlaVar	Tool to evaluate Allan time/variance
cw	continuous wave
ETH	Eidgenössisch Technische Hochschule
FITS	Flexible Image Transport Standard
FPGA	Freely Programmable Gate Array
FPU	Focal Plane Unit
FTP	File Transfer Protocol
FFT	Fast Fourier Transform
LHCP	Left Hand Circular Polarization
NF	Noise Figure
Phoenix-2	Frequency agile spectrometer
Phoenix-3	FFT radio spectrometer
rfi	Radio frequency interference
RHCP	Right Hand Circular Polarization
SFDR	Spurious free dynamic range
sfu	Solar Flux Unit $10^{-26}W/m^2/Hz$
SMA	Small microwave adapter
SNR	Signal to Noise Ratio
SWR	Standing Wave Ratio

Table 6. Acronyms mentioned in labels and comments.

Parameter	value and unit
Frequency range	1GHz ... 5GHz
Channel resolution	61.0KHz
Dynamic range	-100dBm ... -10dBm
Gain control range	50dB min
SFDR	40dB min
Noise figure	15dB max
Allan time intensity	$\geq 100seconds$
Allan time polarization	$\geq 5minutes$
Sampling frequency int. clock	2GS/sec
Channels	2 x 65536
Supply	230Vac, 50Hz
Warm up time	$\geq 15minutes$
Weight	TBD
Dimensions receiver	w=480, h=290, d=440 mm^3

Table 7. Data sheet Phoenix-3 with most important parameters.

References

Hansueli Meyer and Christian Monstein *Mitigation effect of a window function for a FFT spectrometer in an electromagnetic strongly disturbed RF environment*, e-collection report 526, 2007.